Integrated Photonic Ultrasound Transducers for Medical Imaging

Harmsma, Peter J.; van der Heiden, Maurits S.; Altmann, Robert K.; Gerritsma, Anne Maaike; Valappil, Sabiju Valiya; Quesson, Benoit A.J.; Marin, Yisbel E.; Harjanne, Mikko; Bhat, Srivathsa; More Authors

DOI
10.1117/12.3041703

Publication date
2025

Document Version
Final published version

Published in
Integrated Optics

Citation (APA)
Harmsma, P. J., van der Heiden, M. S., Altmann, R. K., Gerritsma, A. M., Valappil, S. V., Quesson, B. A. J., Marin, Y. E., Harjanne, M., Bhat, S., & More Authors (2025). Integrated Photonic Ultrasound Transducers for Medical Imaging. In S. M. Garcia-Blanco, & P. Cheben (Eds.), *Integrated Optics: Devices, Materials, and Technologies XXIX* Article 133690B (Proceedings of SPIE - The International Society for Optical Engineering; Vol. 13369). SPIE. https://doi.org/10.1117/12.3041703

Integrated Photonic Ultrasound Transducers for Medical Imaging

Peter J. Harmsma*[a], Maurits S. van der Heiden[b], Robert K. Altmann[a], Anne Maaike Gerritsma[b], Sabiju Valiya Valappil[c], Benoit A.J. Quesson[b], Yisbel E. Marin[d], Mikko Harjanne[d], Srivathsa Bhat[d], Sami Ylinen[d], Päivi Heimala[d], Anton Stroganov[e], Andreas Frigg[e], Paul L.M.J. van Neer[b]

[a] TNO, Stieltjesweg 1, 2628 CK Delft, The Netherlands; [b] TNO, OudeWaalsdorperweg 63, 2597 AK Den Haag, The Netherlands; [c] Delft University of Technology, Faculty of Applied Sciences, Lorenzweg 1, 2628CJ Delft, The Netherlands; [d] VTT Technical Research Centre of Finland, Tietotie 3, 02150 Espoo, Finland; [e] LIGENTEC SA, EPFL Innovation Park Bâtiment L, Chem. de la Dent d'Oche 1B, 1024 Ecublens, Switzerland

ABSTRACT

We present our experimental results on ultrasound transducers based on Photonic Integrated Circuits. We have fabricated and tested devices based on Mach Zehnder Interferometers and Ring Resonators, in the thick-Silicon On Insulator platform (VTT, Finland) and Si_3N_4 platform (Ligentec, Switzerland). We have obtained a Noise Equivalent Pressure which is two orders of magnitude lower than conventional State-Of-The-Art transducers, clearly demonstrating the huge potential of this concept.

Keywords: Ultrasound, transducer, ring resonator, Mach Zehnder Interferometer, membrane, integrated photonics, noise-equivalent pressure, IPUT.

1. INTRODUCTION

Ultrasound imaging is a powerful technique to retrieve a 3D representation of the interior of an object in general, or of human tissue in medical imaging in particular. An improved Signal to Noise Ratio (SNR) enhances the image quality, which can lead to better diagnosis and improved patient health. Furthermore, a better SNR enables imaging of deeper-lying tissue, as well as an improvement in resolution by allowing the use of higher acoustic frequencies which are more strongly attenuated by the tissue. Peak pressures in patients are regulated for safety reasons, therefore, SNR improvements should follow from improved ultrasound receivers. The state-of-the-art Noise-Equivalent Pressure (NEP) for piezo-based receivers, Capacitive Micromachined Ultrasound Transducers (cMUTs) and Piezoelectric Micromachined Ultrasound Transducers (pMUTs) at acoustic frequencies near 1 MHz is in the order of 0.5 Pa [1][2]. Alternative transducer technologies must be considered to obtain drastic performance improvement. A strong candidate is the Integrated Photonics Ultrasound Transducer (IPUT), in which the ultrasound signal modulates the optical transfer function of a photonic circuit on a membrane. Leinders et.al. [3] reported an IPUT having a NEP of 0.38 Pa at 0.47 MHz and a 21% -6 dB bandwidth. It has a footprint over two orders of magnitude smaller than the acoustic wavelength, so that cascading multiple IPUTs brings the potential of vast NEP reduction. We report on the performance of IPUTs fabricated in two material platforms for Photonic Integrated Circuits (PICs), using either single-membrane or cascaded-membrane configurations, demonstrating superior sensitivity and NEP as compared to state-of-the-art.

2. TRANSDUCER CONCEPT

A schematic of the IPUT is presented in Figure 1. A waveguide-based photonic circuit, in this example a ring resonator, is fabricated on a silicon substrate, with an oxide buffer layer between the substrate and the waveguides. A membrane is formed by etching a hole from the substrate backside. The etching process provides high selectivity between silicon and oxide, such that a clean oxide membrane remains, with the photonic device on top. The membrane mechanical resonance

Integrated Optics: Devices, Materials, and Technologies XXIX, edited by Sonia M. García-Blanco, Pavel Cheben, Proc. of SPIE Vol. 13369, 133690B · © 2025 SPIE
0277-786X · doi: 10.1117/12.3041703

frequency is chosen to match the target acoustic frequency. Deflection of the membrane due to an acoustic signal results in a change in the optical response of the photonic device. The dominant mechanism is the physical elongation of the waveguide. In addition, minor contributions arise from effective index variations caused by waveguide cross-section deformation, and from changes in the material refractive indices via the opto-mechanical stress tensor. Maximum sensitivity is obtained for a circular waveguide having a radius of $R_m/\sqrt{3}$ where R_m is the membrane radius [4]. It should be noted that if a cladding layer is applied on top of the waveguide, in such a way that the waveguide is located at the vertical center of the membrane, the waveguide physical elongation upon membrane deflection is close to zero. Consequently, the sensitivity would be very low. For a homogeneous membrane, the sensitivity scales linearly with the distance between the vertical center of the waveguide and the vertical center of the membrane.

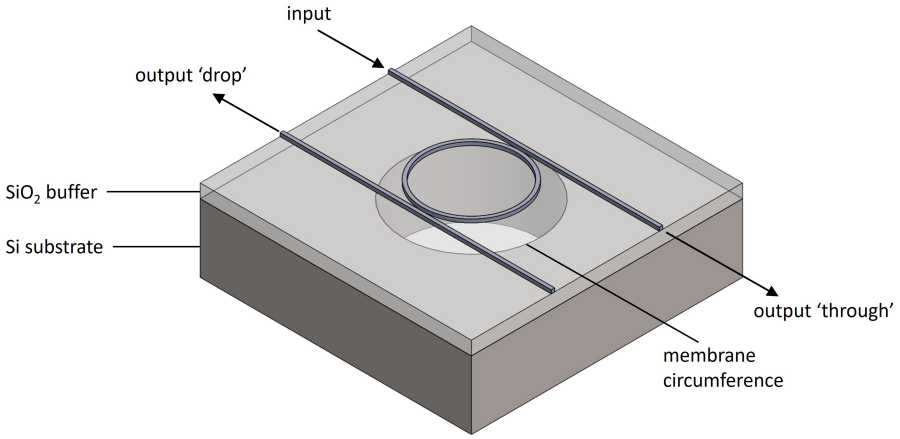

Figure 1: IPUT concept. A waveguide-based photonic circuit, in this example a ring resonator, is located on a mechanical resonator, in this example a membrane. The membrane is formed by local removal of the substrate below the ring resonator by means of a back-side etch. An ultrasound signal (coming from the top) deflects the membrane, leading to a change in the optical transmission.

In case the photonic device is a ring resonator (Figure 2, left), a probe laser is tuned to the wavelength where the slope of the optical resonance is highest. Assuming a Lorentzian resonance shape (a realistic assumption in practice), the maximum slope is at $\lambda = \lambda_{res} \pm \text{FWHM}/(2\sqrt{3})$, where λ_{res} is one of the resonance wavelengths and FWHM is the resonance Full Width Half Max. At this wavelength, the transmission equals 3/4 times the peak transmission. The pressure-induced wavelength shift leads to a transmission change ΔT which can be detected by means of a photodiode. The IPUT response is temperature sensitive, so that the probe wavelength needs to be actively finetuned in case of temperature fluctuations. These fluctuations are at low frequency, and are easily filtered out from the IPUT signal.

Alternatively, a Mach Zehnder Interferometer (MZI) can be applied (Figure 2, center). The sensing arm of the interferometer is routed spiral-wise over the membrane. The path length difference between the sensing arm and the reference arm is chosen small to minimize sensitivity to wavelength noise of the probe laser, but sufficiently large to observe a full interference fringe while scanning the probe laser over a practical wavelength range for performance validation. In our devices we implement a Free Spectral Range (FSR) near 3 nm. We use an MZI with three output waveguides, as has been reported for Fiber Bragg Grating sensing [5] and biosensing [6] applications, providing good sensitivity at any operation point, and quasi-infinite dynamic range due to unambiguous tracking over multiple fringes. In MZI-based IPUTs, multiple membranes can be incorporated in the sensing arm (Figure 2, right), leading to an N-fold sensitivity increase for N membranes, provided that all membranes are located within the area of one acoustic wavelength squared. The amplifier noise, shot noise and acquisition noise increase only slightly with the number of membranes for low-loss waveguides, and dominate the (thermal) noise of the IPUT itself. Consequently, the N-fold sensitivity enhancement leads to a huge improvement in SNR.

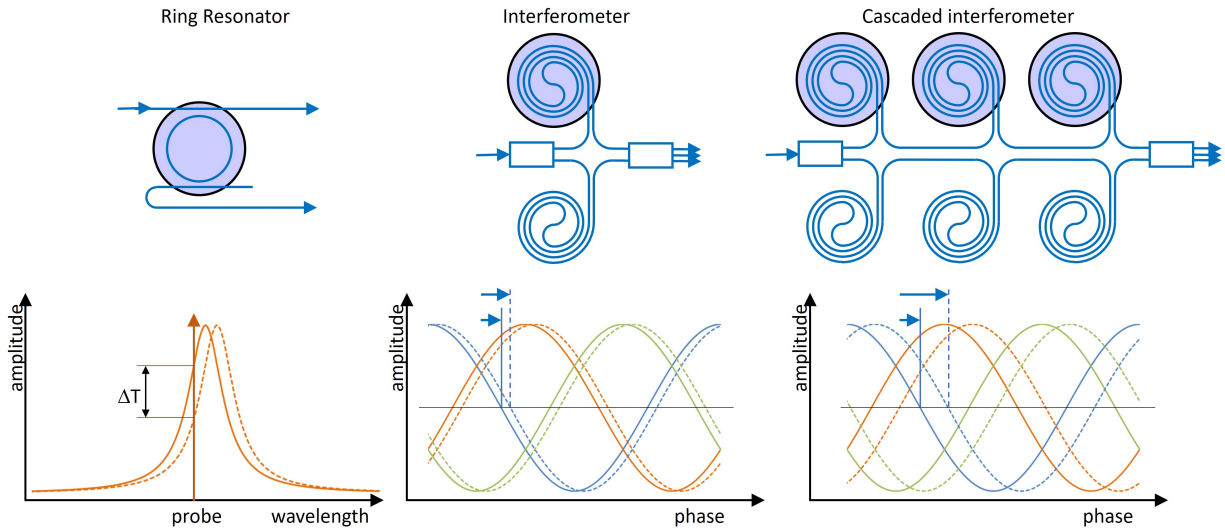

Figure 2: IPUT photonic circuits and their response: ring resonator, MZI and cascaded MZI.

3. DESIGN AND FABRICATION

We employ two material platforms for our IPUT sensors: the thick Silicon On Insulator (SOI) platform of VTT, Finland, and the Silicon Nitride platform of Ligentec, Switzerland. The VTT thick-SOI platform [6] consists of 3 µm thick waveguides, nominal width 1.5 µm for an operating wavelength of 1550 nm. These waveguides are multimode, still, single-mode operation can be achieved by the appropriate use of mode filters and optimized adiabatic transitions. A typical MZI spiral (Figure 3) is designed for minimum excitation of higher-order modes, and maximum transmission of the fundamental TE-polarized mode. In the MZI, mode filters are applied to both arms prior to recombining these in the output coupler. The nominal thickness of the silicon dioxide buffer layer which forms the membrane is 3 µm before device fabrication. We explored different process flows, leading to either a thinner membrane (down to 2.6 µm due to prolonged back side etching) or a thicker membrane (up to 3.2 µm due to oxide deposition). A membrane radius of 55 µm is chosen to obtain an acoustic resonance frequency near 1 MHz, as appropriate for ultrasound medical imaging. Note that this is the minimum achievable membrane radius, and thus the highest acoustical frequency for this membrane thickness, due to the minimum bending radius of the waveguide.

Ring resonators-based IPUTs require high optical Q-factors, which in turn require the use of directional couplers. The thick-SOI platform does not support directional couplers based on strip waveguides (which are required for small bending radii) due to the strong confinement of the optical field in the strip waveguide. Therefore, ring resonator based IPUTs were fabricated in the Ligentec AN800 platform comprising 800 nm thick Si_3N_4 waveguides with a nominal width of 1 µm for an operating wavelength of 1550 nm. The membrane thickness in this case is 11.4 µm, much thicker than the 3 µm thick-SOI membranes. As thicker membranes have higher mechanical resonance frequencies, we increased the nominal membrane radius to 91 µm aiming for a 2 MHz acoustic resonance frequency. Again, membranes were defined by means of a back-side etch through the substrate. For the standard Si_3N_4 layer stack, the distance of the waveguide layer to the vertical center of the membrane is 1.3 um, which is smaller than in the thick-SOI platform (4.5 µm). In future iterations, deviations from the standard can be considered to mitigate the associated reduction in sensitivity.

Figure 4 shows examples of fabricated devices. The chips were assembled onto an acoustic backing material to suppress acoustic reflections, after which two 32-channel polarization maintaining fiber arrays were attached on orthogonal facets to address a variety of devices.

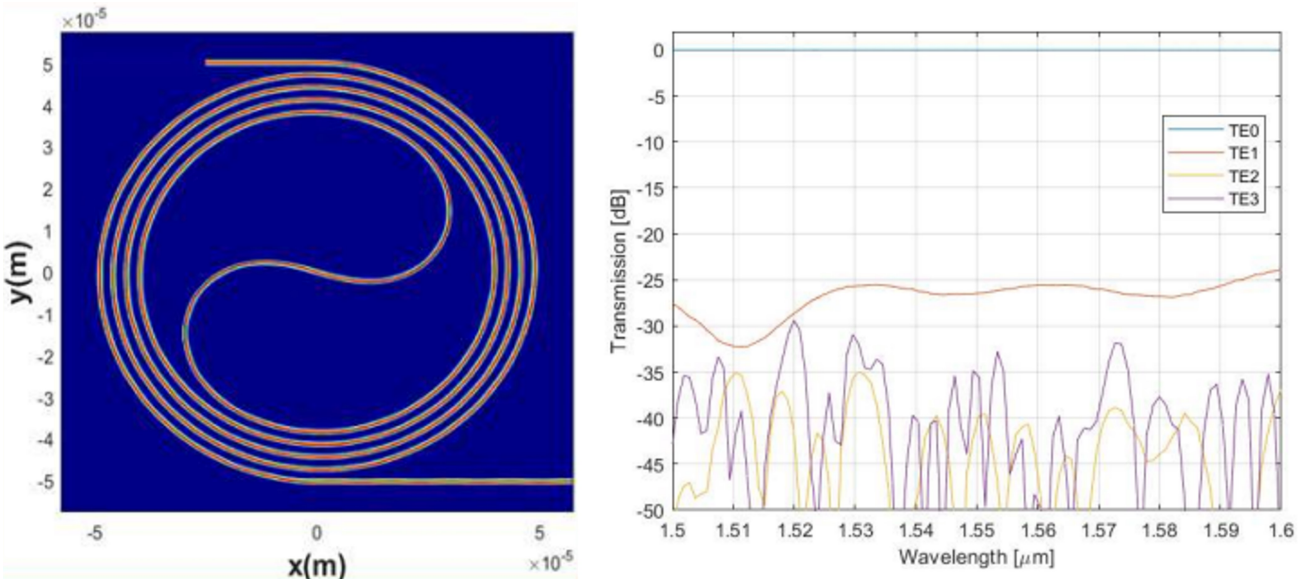

Figure 3: Left: a waveguide spiral is designed to fit on the membrane. Euler bends are applied to reduce the area occupied by the turning point while maintaining high optical transmission. Right: simulated optical transmission of the spiral. The spiral is optimized for maximum transmission of the fundamental TE-polarized mode, and minimum excitation of higher-order modes.

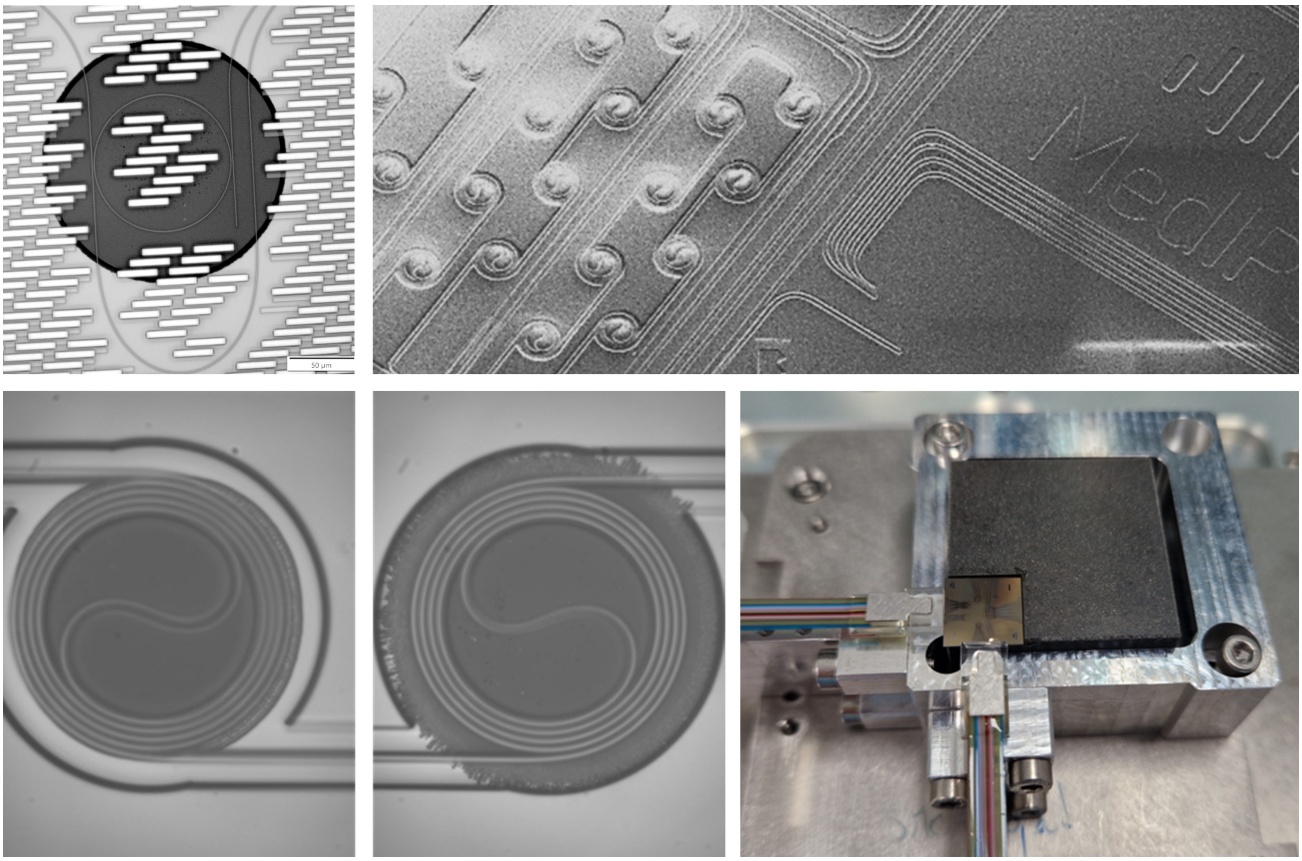

Figure 4: Fabricated devices: Ligentec Si_3N_4 ring resonator on a membrane (top left); VTT thick-SOI IPUTs: SEM birds-eye-view of an array of membranes (top right) and microscope images (lower left and center); packaged chip with 2 x 32-channel fiber array on acoustic backing (lower right).

4. EXPERIMENTAL RESULTS

Typical optical transmission spectra are presented in Figure 5. The wavelength sweeps in the left graph show the three (thick-SOI) MZI outputs at their characteristic 120° phase difference. In a preparatory iteration we observed considerable degradation of interference quality for MZIs comprising more than 7 spirals. In this work, we addressed this by including mode filters in the sensing and reference arms to prevent higher-order modes from entering the output coupler of the MZI, as well as by optimizing the S-bend design of the spiral (Figure 3). The center graph in Figure 5 relates to a 20-membrane MZI, with mostly bands of excellent interference, a clear proof that this approach indeed leads to substantial improvement. The rightmost graph shows the through- and drop port of a Si_3N_4 ring resonator having an optical Q-factor well above 100,000.

During acoustic tests, the entire assembly is positioned up-side-down in a water tank, with a calibrated acoustic source below (Imasonic 13579, 250 kHz or Panametrics V303, 1 MHz). The distance between chip and transducer is 27 cm, so that the chip is essentially in the acoustic far field of the transducer. In this work, we use only one output of the MZI. The wavelength of a tunable laser (EXFO T100S-HP) is set to observe maximum sensitivity. The device outputs are recorded by means of photo diodes (Thorlabs DET10C2), Trans Impedance Amplifiers (FEMTO DHPCA-100 and in-house built) and a digitizer system (Spectrum M2i.4964-exp,16 bit, 8x30 MS/s). We excited the transducer by means of a single-cycle sine, providing a broadband acoustic spectrum, and recorded 1000 traces. The IPUT acoustic bandwidth is obtained from the 1000-fold averaged signal, the NEP relates to a single trace.

We reduced the transmitter voltage to progressively lower voltages to find the NEP. For a thick-SOI MZI with 5 membranes we obtained a NEP of only 0.0043 Pa at 540 kHz. This is approximately two orders of magnitude below the state-of-the art [1][2] and previously reported IPUTs [3], clearly demonstrating the potentially disruptive opportunities of IPUTs. For practical purposes, we adhere to a 4 times larger NEP than the theoretical definition in which the signal amplitude equals the noise amplitude, leading to a $NEP_{practical}$ of 0.017 Pa (yellow line in the left graph of Figure 6). Our acoustic -6 dB bandwidth is 13%. In our further work we will explore various strategies to enlarge the bandwidth. Note that the peak sensitivity is obtained at a lower frequency than the target 1 MHz, we attribute this to a thinner membrane (2.6 µm in this case), a slightly larger membrane radius than designed (Figure 4, lower center), and the influence of mechanical prestress in the membrane which is an intrinsic property of SOI wafers. The right-hand graph in Figure 6 shows that the sensitivity expressed in physical waveguide elongation per unit pressure scales linearly with the number of membranes, which indicates that higher sensitivity and lower NEP are well possible. The NEP of the Si_3N_4 ring resonator based IPUTs is relatively poor, for two reasons: 1) the ring resonators cannot be cascaded as conveniently as MZIs, and 2) in these devices the waveguides are close to the vertical center of the membrane.

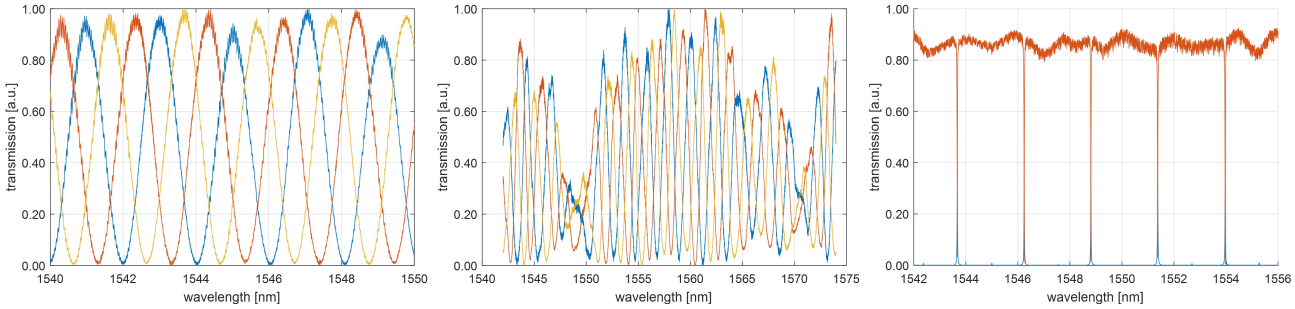

Figure 5: Optical transmission of thick-SOI MZIs with 8 (left) and 20 (center) spirals; Si_3N_4 Ring Resonator with Q-factor 100,000 (right).

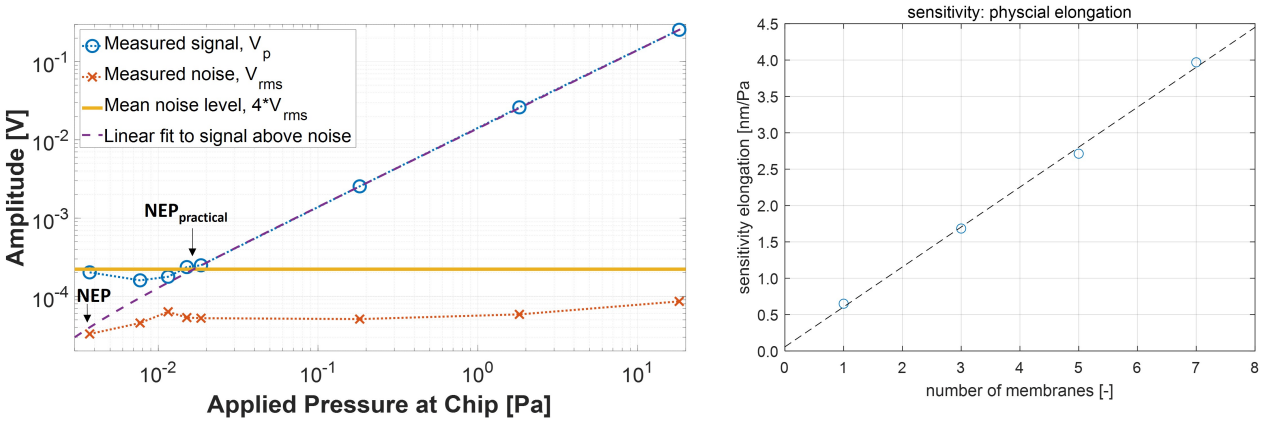

Figure 6: Noise Equivalent Pressure (left) and linearity of sensitivity with number of membranes (right), data for thick-SOI MZI chip.

Table 1: Key performance parameters of ultrasound receivers, comparing the State Of The Art conventional transducers to Integrated Photonic Ultrasound Transducers ([3][7], this work).

	SOTA [1][2]	**Leinders et al. [3]**	**Ouyang et al. [7]**	**TNO 5 cascaded**
Type	Piezo/cMUT/pMUT	RR IPUT	MZI IPUT	MZI IPUT
NEP [Pa]	0.50	0.40	0.38	0.0043
NEP practical [Pa]	2.0	1.60	1.52	0.017
Center frequency [MHz]	1	0.76	0.47	0.54
-6 dB bandwidth [%]	80	19	21	13

5. CONCLUSIONS AND OUTLOOK

We have demonstrated ultrasound receivers based on Photonic Integrated Circuits. The Noise Equivalent Pressure of a 5-membrane device is approximately two orders of magnitude below the State Of The Art conventional transducers. Due to the small membrane size as compared to the acoustic wavelength, a higher number of cascades is possible while maintaining good optical performance, and we will explore a further reduction in NEP by increasing the number of membranes in a single device. The acoustic bandwidth is yet narrow, this will be addressed in future work. The thick-SOI platform is based on a fairly thin membrane (3 μm), leading to relatively low acoustic frequencies (1 MHz) whereas the Si_3N_4 platform with a thicker membrane (> 10 μm) can support higher acoustic frequencies. We believe that the choice of platform (SOI - Si_3N_4) and circuit (MZI – ring resonator) is highly application-dependent, and we will continue to explore the parameter space in IPUT design for optimal performance. The demonstrated NEP improvement clearly shows the huge potential for this technology in ultrasound transducers.

ACKNOWLEDGEMENTS

We kindly express our gratitude towards all partners in the MedIPUT project: VTT (Finland), Ligentec (Switzerland), EIBIR (Austria) and Vermon (France). We highly appreciate the help of our colleagues Floris Nyendaal, Michiel Oderwald, Arjen Amelink, Erwin Boer, Raymond Vollebregt, Jan Kuijt, Mercedes Alcon Camas, Frank Klaassen, Dinah Brander, Daniele Piras and Rob Jansen for their support in discussions, device assembly and testing. Moreover, we'd like to thank Martin Verweij and Emile Noothout (Delft University of Technology, The Netherlands) and Sander Dorrestein

(CITC, The Netherlands) for their valuable contributions. This work was supported by the TNO Early Research Program (ERP) ‘Opto-acoustics’, NWO grant NWA 1160.18.095 ‘Opto-acoustic sensor and ultrasonic microbubbles for dosimetry in proton therapy’, and partly funded by the European Union, MedIPUT project, HORIZON-CL4-2022-DIGITAL-EMERGING-01, Grant 101092947, https://med-iput.eu/.

- Corresponding author: peter.harmsma@tno.nl; phone +31 (0)611 382 300; https://www.tno.nl

REFERENCES

[1] Xia, W., Piras, D., van Hespen, J.C.G., van Veldhoven, S., Prins, C., van Leeuwen, T.G., Steenbergen, W. and Manohar, S. (2013), An optimized ultrasound detector for photoacoustic breast tomography. Med. Phys., 40: 032901. https://doi.org/10.1118/1.4792462 R. Manwar, et. al., "Overview of Ultrasound Detection Technologies for Photoacoustic Imaging," Micromachines, vol. 11, no. 7, p. 692, 2020

[2] Afshin Kashani Ilkhechi, Christopher Ceroici, Zhenhao Li, and Roger Zemp, "Transparent capacitive micromachined ultrasonic transducer (CMUT) arrays for real-time photoacoustic applications," Opt. Express 28, 13750-13760 (2020)

[3] Leinders, S., Westerveld, W., Pozo, J. et al. A sensitive optical micro-machined ultrasound sensor (OMUS) based on a silicon photonic ring resonator on an acoustical membrane. Sci Rep 5, 14328 (2015). https://doi.org/10.1038/srep14328

[4] Véronique Rochus, Roelof Jansen, Jeroen Goyvaerts, Peter Neutens, John O'Callaghan, and Xavier Rottenberg, “Fast Analytical model of MZI Micro-opto-Mechanical Pressure Sensor”. Journal of Micromechanics and Microengineering. 28. 10.1088/1361-6439/aab461 (2018).

[5] M. Perry, P. Orr, P. Niewczas and M. Johnston, "High-Speed Interferometric FBG Interrogator With Dynamic and Absolute Wavelength Measurement Capability," in *Journal of Lightwave Technology*, vol. 31, no. 17, pp. 2897-2903, Sept.1, 2013, doi: 10.1109/JLT.2013.2276391

[6] R. J. J. van Gulik, B. M. de Boer and P. J. Harmsma, "Refractive Index Sensing Using a Three-Port Interferometer and Comparison With Ring Resonators," in IEEE Journal of Selected Topics in Quantum Electronics, vol. 23, no. 2, pp. 433-439, March-April 2017, Art no. 8200207, doi: 10.1109/JSTQE.2016.2601899.

[7] Cherchi, M., Bera, A., Kemppinen, A., Nissilä, J., Tappura, K., Caputo, M., Lehtimäki, L., Lehtinen, J., Govenius, J., Hassinen, T., Prunnila, M., & Aalto, T. (2023). Supporting quantum technologies with an ultralow-loss silicon photonics platform. Advanced Photonics Nexus, 2(2), Article 024002. https://doi.org/10.1117/1.APN.2.2.024002

[8] Boling Ouyang, Yanlu Li, Marten Kruidhof, Roland Horsten, Koen W. A. van Dongen, and Jacob Caro, "On-chip silicon Mach–Zehnder interferometer sensor for ultrasound detection," Opt. Lett. 44, 1928-1931 (2019)

[9] Westerveld, W.J., Mahmud-Ul-Hasan, M., Shnaiderman, R. et al. Sensitive, small, broadband and scalable optomechanical ultrasound sensor in silicon photonics. Nat. Photonics 15, 341–345 (2021). https://doi.org/10.1038/s41566-021-00776-0